Complications in Addressing Liquefaction Vulnerability in Stratified Soils from Building to Cluster to Community

Shideh Dashti i), Yu-Wei Hwang ii) and Caroline Bessette iii)

- i) Associate Professor, Department of Civil, Environmental, and Architectural Engineering, University of Colorado Boulder, Boulder, CO 80309, U.S.
- ii) Assistant Professor, Department of Civil Engineering, National Yang Ming Chiao Tung University, Hsinchu, Taiwan 300 iii) Ph.D Student, Department of Civil, Environmental, and Architectural Engineering, University of Colorado Boulder, Boulder, CO 80309, U.S.

ABSTRACT

The existing engineering methodologies for liquefaction mitigation rely on free-field triggering in uniformly layered granular soil deposits. These methods routinely ignore cross-layer interactions in stratified deposits, consequences of softening and various mechanisms of mitigation on building performance, or interactions between and among structures in close proximity of each other. In this paper, through an experimental-numerical study, we show that these methods are unreliable, jeopardizing our ability to assess and mitigate liquefaction vulnerability from building to cluster, and to community scales. Fully-coupled, 3D, dynamic finite element analyses, validated with centrifuge experiments, show that combining ground reinforcement with drainage and densification (e.g., through installation of dense granular columns) can improve foundation's settlement, but not necessarily to acceptable levels. To achieve desired levels of reduction in settlement, it is critical to minimize the likelihood of clogging in such drains, particularly in the presence of silt interlayers. These methods, however, may increase foundation's tilt potential, which must be evaluated on a case-by-case basis. Unsatisfactory tilt is often uneconomical to repair, which may lead to the decision to demolish or relocate. And this engineering demand parameter (EDP) becomes particularly difficult to improve in urban settings and in stratified and non-uniform deposits. The combined influence if seismic coupling and stratigraphic variability on mitigation efficacy is shown to be significant in terms of foundation tilt, spectral accelerations, and flexural drifts experienced within the superstructure of both mitigated and unmitigated neighbors. These effects are notable for spacing-to-foundation width-ratios (S/W) as large as 1.0, which are common in cities. Additional measures and technologies may be needed to reduce tilt to acceptable levels in closely-spaced cluster configurations and realistically stratified deposits, while simultaneously strengthening both the ground and structures at an area-level and in a cost-effective and sustainable manner.

Keywords: liquefaction, centrifuge modeling, numerical modeling, seismic coupling, soil-structure interaction, structure-soil-structure interaction, community resilience, mitigation.

1 INTRODUCTION

Historically, seismic liquefaction has not contributed significantly to casualties (with the exception of liquefaction-induced landslides). However, the short-and long-term socio-economic impacts of seismic liquefaction have been significant. Liquefaction has repeatedly disrupted aid and recovery for years following the event through damage to ports, lifelines, and housing. Simultaneously, liquefaction recovery and remediation efforts following an earthquake have displaced communities, with severe implications on financial, social, physical, and mental health (Balachandran et al. 2021). Figure 1 shows a series of socioeconomic factors (Dashti et al. 2022; Cabas et al. 2023), including population density, transport

infrastructure, and annual income, interconnected with a range of geotechnical hazards, including landslides, liquefaction potential, and the intensity spatial distribution corresponding to the 2021 Nippes, Haiti Earthquake as an example. The highest population density, the lowest income level, the highest risk of soil liquefaction (where we also found evidence of liquefaction during reconnaissance), and the highest earthquake intensity overlapped in the southern region of Haiti, compromising the most marginalized urban areas (e.g., Les Cayes). In such situations, the impacts of hazards like liquefaction on recovery, aid, and population displacement may be disproportionately felt by the most marginalized segments of society.

Due to the universally severe impacts of community relocation in areas with likelihood of seismic

liquefaction, it is critical for practitioners and the public to reliably assess the engineering and financial implications of mitigation at an area-wide level. The existing engineering methodologies for liquefaction mitigation are primarily based on triggering in the freefield, without properly accounting for cross-layer interactions in stratified profiles or the consequences on and interactions between structure(s), making them unreliable particularly in urban settings. Unreliable estimations of hazard and consequence tamper reliable impact-based risk estimation, advocacy, decision making, and policy that support effective liquefaction mitigation. This leaves many major cities and their most marginalized communities, including those in Tokyo, Vancouver, San Francisco, Santiago, and Jakarta, vulnerable to extensive liquefaction related damage or community relocation, such as experienced in Christchurch during the 2010-11 earthquake series (Cubrinovski 2017; Balachandran et al. 2021).

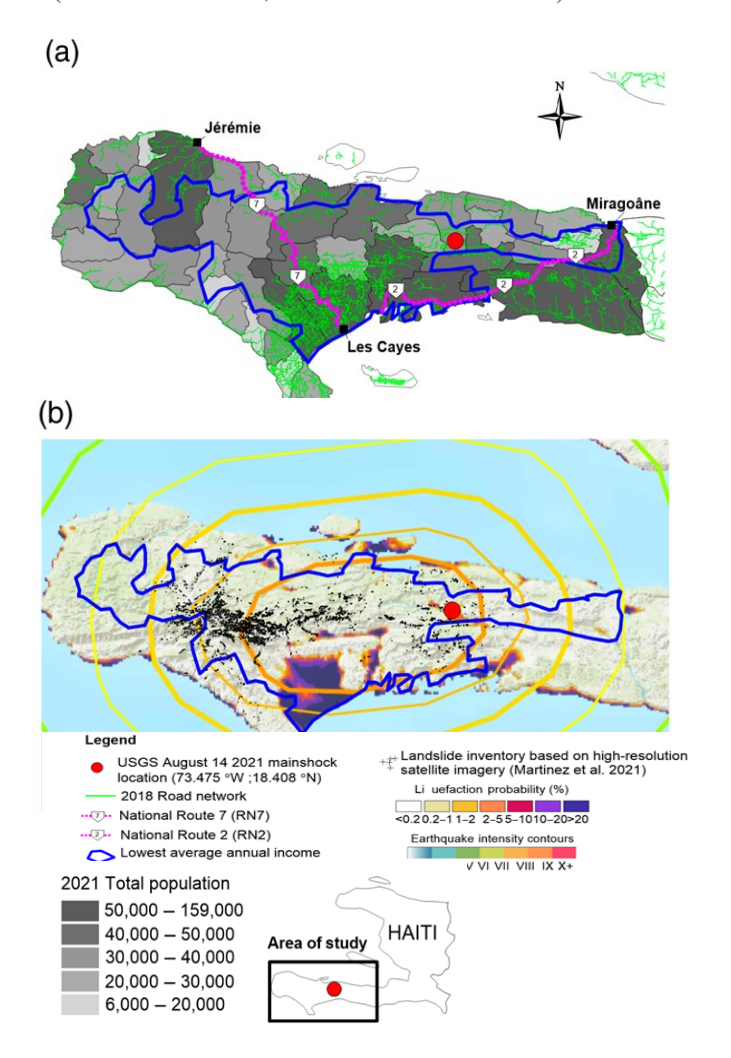


Fig. 1. Intersectional maps depicting: (a) 2021 population map with the boundary of the lowest average annual income within the study region in Haiti. The road network map is also shown highlighting important lifelines such as National Route 7 (RN7), which was affected after the 2021 earthquake. (b) The USGS liquefaction probability map, earthquake intensity contours of the

2021 Nippes earthquake, and a landslide inventory map overlaid on the boundary of the lowest average annual income (figure from Cabas et al. 2023).

Recent case histories as well as experimental and numerical studies have demonstrated that methods for liquefaction triggering, consequence, and mitigation in the free-field do not apply to buildings on shallow foundations (e.g., Dashti et al. 2010a,b; Bullock et al. 2019a,b) because of differing seismic demands, deformations, and flow patterns. Much effort has been directed toward improving our understanding of soil-structure interaction (SSI) and structure-soil-structure interaction (SSSI) on uniformly layered deposits of liquefiable clean sand with or without mitigation (Dashti et al. 2010a,b; Hausler 2002; Karimi & Dashti 2016; Karimi et al. 2018; Olarte et al. 2017; Bullock et al. 2019a,b; Kirkwood and Dashti 2019; Hwang et al. 2021).

Though insightful in demonstrating the critical importance of SSI and SSSI, saturated granular deposits in the field susceptible to liquefaction often have non-uniform stratification and uncertain layer continuity, including low-permeability silt or clay layers (Ishihara 1985; Kokusho and Fujita 2001; Badanagki et al. 2019). Previous studies have revealed that liquefaction-induced lateral spreading can manifest even in slopes with inclinations as gentle as 0.3-1°, resulting in substantial displacements of up to 2 m and posing risks to critical infrastructure and lifelines (O'Rourke and Lane 1989). It is unclear how variations in soil layer thickness (a buried slope) may induce lateral deformations in a liquefiable site and how that would impact structures on shallow foundations, particularly after remediation.

Additionally, the severity of liquefaction manifestation can be strongly influenced, if not controlled, by interactions among soil layers, as demonstrated during the 2010-2011 earthquake sequence in Christchurch, New Zealand (Cubrinovski 2017). Beyzaei et al. (2018) showed the significance of stratification in natural deposits with thin silt interlayers that can lead to abrupt changes in permeability, affecting the continuity of critical layers, soil ejecta formation, and the overall surface manifestations of liquefaction. Several laboratory experiments and numerical studies have also shown that spatial variability within soil profiles can impact lateral and vertical ground deformations, shear or volumetric strains, the formation of surface ejecta, and the damage to inelastic structures (Dashti et al. 2010b; Cubrinovski et al. 2017; Luque and Bray 2017; Badanagki et al. 2018; Paramasivam et al. 2019). These system-level effects are poorly understood and are not included in existing triggering and settlement procedures that assume uniformly layered and level deposits of clean sand. Hence, they are also not included in designing mitigation strategies. The next generation of liquefaction mitigation methodologies need to account for complexities associated with SSI, SSSI, and

stratigraphic variability.

In this paper, our goal is to set the stage for more reliable and effective engineering solutions to liquefaction vulnerability at a systems level, from building to cluster and to community scales. We first evaluate the capabilities and limitations of 3D solidfluid, fully-coupled, nonlinear, effective-stress, dynamic finite-element analyses with a state-of-the-art soil constitutive model in capturing the seismic response of stratified liquefiable deposits and structures mitigated with dense granular columns (DGCs) as an example of ground remediation. This comparison is made against a large range of centrifuge experimental results that include various degrees of stratification. This evaluation incorporates varying soil stratigraphic conditions and isolated different mitigation mechanisms offered by (drainage, reinforcement, and installation-DGCs induced densification). Subsequently, through a limited numerical sensitivity study, we investigate how DGC mitigation properties, stratigraphic variability, building properties, and seismic coupling between neighboring structures impact the effectiveness of DGCs on critical engineering demand parameters (EDP) of interest for the soil-foundation-structure system. The results are intended to shed light on the complexities associated with liquefaction mitigation in realistic sites, guiding future remediation design in urban settings.

2 CENTRIFUGE AND NUMERICAL MODELING

A series of centrifuge experiments were conducted at the University of Colorado Boulder's (CU) 5.5 m-radius, 400 g-ton centrifuge facility to evaluate seismic site response, SSI, SSSI, and soil-embankment interaction on layered liquefiable soils with dense granular columns (DGCs) or other forms of drainage as mitigation (e.g., Badanagki et al. 2018-2019; Kirkwood and Dashti 2018a,b; Tiznado et al. 2020). In this paper, we use their results to validate numerical simulations. The sequence of experiments involving one isolated structure or embankment is first shown in Fig. 2, which enables evaluation of stratigraphic changes in soil and mitigation mechanisms provided by DGCs on the seismic performance of geotechnical or building structures.

As shown in Fig. 2, these tests examined the response of a free-field (FF) layered deposit without any treatment (Test FF_{NM}), a single DGC within a layered, free-field liquefiable deposit (Test FF_{RF-DR} , where RF and DR indicate the "reinforcement" and "drainage" mechanisms of mitigation, respectively), and a series of tests involving an embankment or a shallow-founded structure untreated or treated with DGCs. The embankment tests were designed to explore the relative significance of different mitigation mechanisms compared to a case with no mitigation (Test EM_{NM}): i) reinforcement and enhanced drainage (Test EM_{RF-DR}); ii)

reinforcement with inhibited drainage with latex membrane (Test EM_{RF}); iii) reinforcement with inhibited drainage combined with densification (Test EM_{RF-DS}). Additionally, Test ST_{NM} examined an untreated structure [e.g., labeled as "Structure A" representing a 3-story building on a mat foundation]. Finally, Test ST-NU_{NM} or ST-NU_{RF-DR} involved a non-uniform (NU) liquefiable layer with two Structures A separated by a distance of 3.5 their foundation width. In this experiment, one of the structures was unmitigated, and the other was treated with draining DGCs (providing RF-DR mitigation).

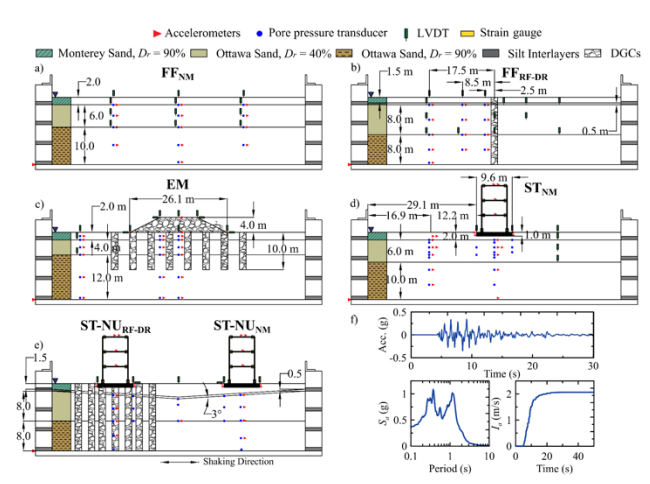


Fig. 2. Configuration and instrumentation layout of the centrifuge experiments (all units are in prototype scale, meters): a) Test FF_{NM}, free-field and no mitigation (Kirkwood and Dashti 2018); b) Test FF_{RF-DR}, single-drain (Badanagki et al. 2018); c) Tests EM_{NM}, EM_{RF-DR}, EM_{RF-DS}, and EM_{RF}, representing experiments with an embankment with DGCs (Tiznado et al. 2020); d) Test ST_{NM}, isolated Structure A (Bessette et al. 2022); e) Test ST-NU_{NM} and ST-NU_{RF-DR} (NU for "non-uniform"), involving two separated Structures A on a non-uniform liquefiable soil profile (Badanagki et al. 2019) [NM for "no mitigation", RF-DR for "reinforcement and drainage", RF for "reinforcement with inhibited drainage", & RF-DS "reinforcement, inhibited drainage. for densification"]; and f) Mean acceleration and Arias Intensity (Ia) time histories, and 5%-damped acceleration response spectra (S_a) of the first major motion recorded in all tests, Kobe-L.

In all test scenarios, the soil profile configurations consisted of a dense Ottawa F65 sand layer ($D_{50} = 0.15$ mm, $c_u = 1.56$, $e_{min} = 0.53$, $e_{max} = 0.81$ [Olarte et al. 2017]) dry pluviated at a relative density (D_r) of approximately 90% at the bottom, overlaid by loose Ottawa sand with $D_r \approx 40\%$ in the middle, and a 2-m thick layer of dense Monterey 0/30 sand ($D_{50} = 0.40$ mm, $c_u = 1.30$, $e_{min} = 0.54$, $e_{max} = 0.84$ [Dashti et al. 2010a]) at a D_r » 85% as a dense, draining crust. In all tests, the groundwater table was located at the surface. While this general soil profile configuration remained consistent across all tests, the thickness of Ottawa sand was varied. In Tests FF_{RF-DR} and ST-NU, a thin Silica silt layer (0.5 m thick) was included to create a low permeability cap above loose Ottawa sand. In Test ST-NU, the nonuniform liquefiable layer was prepared with its upper boundary sloped at 3°.

In Tests ST_{NM} and ST-NU, a 3-story moment-resisting steel frame simplified as a 3-degree-of-freedom (DOF) model (Structure A, detailed in Fig. 3c) was placed on a 1 m-thick mat foundation, as shown in Figs. 2b and 3b. To account for concentrated nonlinear and inelastic deformations, replaceable fuses were placed at the structure's beam and column ends (Olarte et al. 2017).

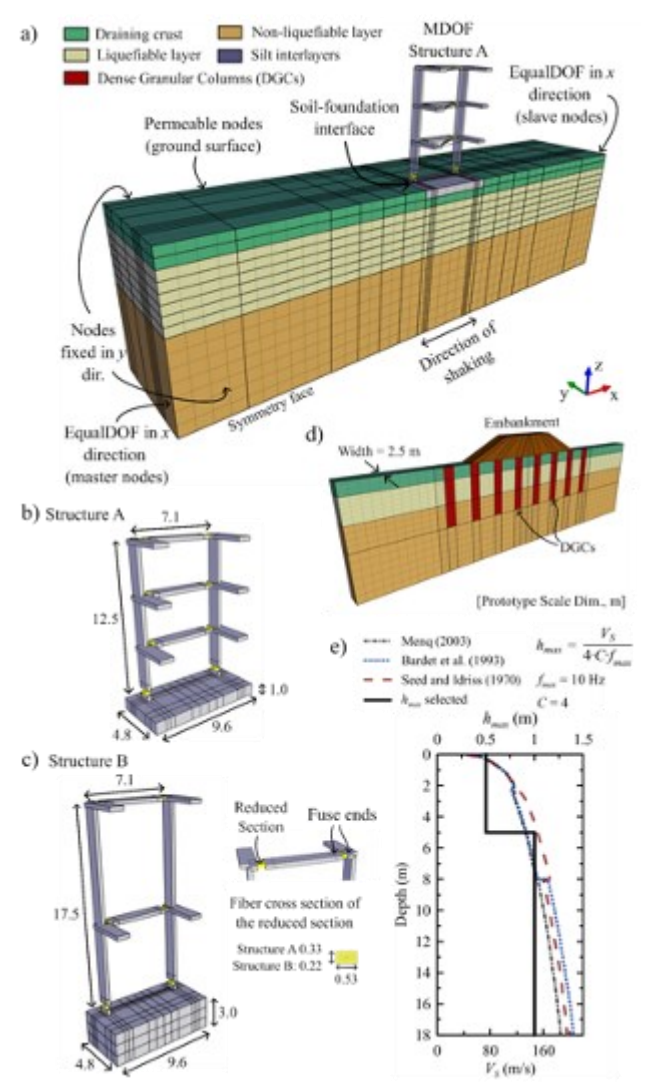


Fig. 3. a) Schematic of the numerical simulation of Test ST_{NM}, with Structure A, as a representative case, with the assigned boundary conditions; b-c) 3D view of Structures A and B (Note that Structure B is only used in the numerical sensitivity studies), their foundations, and structural fuse details; d) Schematic of the numerical simulation of Tests EM with an embankment and DGC configurations; and e) V_s profiles [using empirical procedures from Seed and Idriss (1970), Bardet et al. (1993), and Menq (2003)] and selection of element size distribution for Test ST_{NM} (all units are in prototype scale meters).

In the experiments involving mitigation, the DGC diameter was 1.75 m and placed at a center-to-center spacing of 4.9 m, resulting in an area replacement ratio (A_r) , defined as the area of the granular columns to the total treatment area in plan view) of 10%. DGCs were constructed within closed-end geotextile filters in each test to prevent clogging during consecutive shaking. In

the tests that isolated the contribution of drainage (e.g., Test EM_{RF}), a thin latex membrane (0.2 mm thick) was placed around the DGCs to inhibit drainage within the column. In Test EM_{RF-DS}, the drainage was inhibited through columns by a latex membrane, while the surrounding soil was also pluviated at a denser state, with a D_r of 90%. Tests EM modeled a 4-m high granular embankment with side slopes of 2H:1V on top of the liquefiable soil profile. The material representing granular columns and the embankment consisted of relatively uniform, clean, fine gravel ($D_{50} = 2.50$ mm, $c_u = 1.54$, $e_{min} = 0.54$, $e_{max} = 0.92$ [Badanagki et al. 2018]).

All selected experiments used a flexible-shear-beam (FSB) container to minimize boundary effects. The models were subject to a centrifugal acceleration of 70 g. Subsequently, a servo-hydraulic shake table was employed to apply a series of one-dimensional (1D) horizontal ground motions to the base of the container during flight. For numerical validation, we used the experimental results recorded during the first major motion (identified as Kobe-L) with a peak ground acceleration (PGA) of 0.35 g. Fig. 2c displays the mean acceleration time history, 5%-damped acceleration response spectrum (S_a), and the Arias Intensity (I_a) time history of the Kobe-L motion recorded at the base of the container.

Three-dimensional (3D), fully-coupled, effective stress, nonlinear finite element (FE) simulations were object-oriented, within the performed computation platform OpenSEES (Mazzoni et al. 2006) on the Alpine supercomputer at CU. These simulations were first validated with the presented centrifuge experiments and then expanded with additional input parameters. To model the nonlinear response of the granular soil layers, we used the pressure-dependent, multi-yield surface, version 2, soil constitutive model (PDMY02) implemented in OpenSEES (Elgamal et al. 2002). A small-strain Rayleigh damping value of 3% at frequencies corresponding to the soil column's first and third initial modes was used in addition to the model's hysteresis damping, following a similar methodology adopted in Hwang et al. (2021, 2022), Ramirez et al. (2018).

Best-fitted parameters were calibrated to capture: (1) the fully drained or undrained monotonic and cyclic triaxial element tests; (2) the empirical cyclic stress ratio (CSR) relationships to trigger liquefaction in 15 cycles (NCEER 1997); and (3) site response in a previous free-field boundary-value centrifuge test involving the same soil column and sequence of motions (Hwang et al. 2021). The DGC and embankment material properties were determined by Tiznado et al. (2020) based on: (1) recommendations from Rayamajhi et al. (2016a,b) to align with empirical design correlations; and (2) results from strength and permeability tests conducted by Badanagki et al. (2018) and Li et al. (2018).

All soil elements were represented with two-phase

materials (solid and fluid) and modeled using 3D, higher-order (20-8) brick elements with the u-p formulation. In the u-p formulation, all corner nodes of the elements had 4 degrees-of-freedom (DOFs), three for solid displacement and one for fluid pressure. The other nodes had 3DOFs for displacement alone. The fluid bulk modulus at atmospheric pressure was set to 2×10⁶ kPa.

Fig. 3 shows a schematic drawing of a representative model (e.g., Test ST_{NM}) with the assigned boundary conditions, shear-wave velocity (V_S) profiles, and selected element size distribution. For mitigated models, the nodes of DGCs and their surrounding soil elements were assumed to be tied together (i.e., no interface elements or relative displacement). In Tests FF and ST, only half of the physical models were represented numerically, based on symmetry along the axis perpendicular to the shaking direction (i.e., y), Fig. 3a.

For Tests EM, we modeled a representative DGC tributary area within the container, which had a width of 2.5 m, taking advantage of the regular arrangement of DGCs and the embankment in the y-direction, Fig. 3d. For the tests involving a building model, 20-8 node brick elements with the u-p formulation were used to model the foundation. The foundation was allowed to move relative to the soil, as the lateral nodes were only fixed in the two horizontal directions (i.e., x-y) (following Hwang et al. 2021, 2022]. The structural elements were assigned a damping ratio of 0.2% with Rayleigh damping based on the measured (experimental) damping from the structure (Olarte et al. 2017).

Fig. 4 compares the experimental and numerical results for all tests involving an isolated structure or embankment with or without mitigation in terms of peak EPWP beneath the center of the foundation (middle of the liquefiable layer and dense layer), PGA (middle of the liquefiable and dense layers and on the foundation) or peak roof acceleration (PRA), roof S_a at the corresponding structure's fundamental mode $[S_a(T_{o,Str})]$, permanent foundation settlement or cumulative vertical displacement at the bottom of the embankment along its centerline (D_v) , permanent foundation tilt (q), and permanent or peak transient lateral displacement of the foundation or embankment (D_h) in cases where reliable experimental recordings were available. Fig. 5 compares a subset of similar results for the case of two adjacent structures like A, with no mitigation and with drains around the perimeter of one.

In summary, despite the known limitations and challenges in the centrifuge tests used for validation, overall, the numerical simulations provided reasonable predictions of permanent structural or embankment settlement, lateral displacement or rotation, amplitude, and rate of excess pore pressure generation, and peak accelerations on layered, stratified, highly nonlinear, liquefiable granular deposits with varying mitigation mechanisms provided by DGCs. It is well known that a continuum framework, particularly the PDMY02 model,

poorly predicts volumetric deformations due to sedimentation. Neither can these simulations capture the formation and movement of sand ejecta. However, these shortcomings are expected to have a smaller impact in cases involving mitigation near structures (evident through smaller differences).

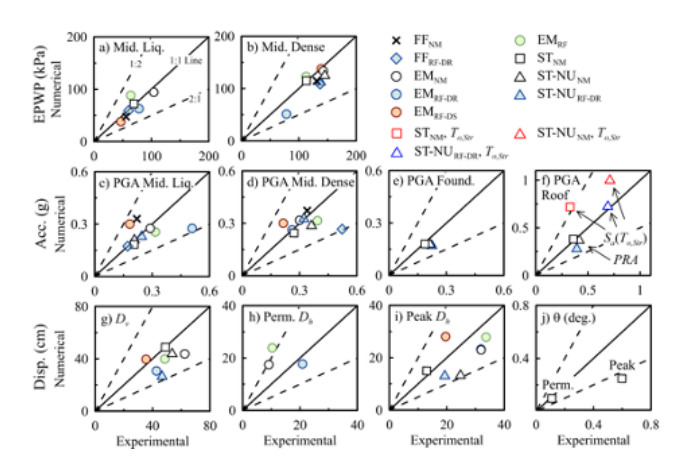


Fig. 4. Comparison of experimentally measured and numerically computed excess pore water pressures (EPWP) in: a) the middle of the liquefiable layer; and b) the middle of the dense layer; comparison of PGAs: c) in the middle of the liquefiable layer; d) in the middle of dense layer; e) on the foundation; f) peak roof acceleration (PRA) and S_a at the structure's fundamental period $[S_a(T_{o,Str})]$; g) permanent foundation settlement or cumulative vertical displacement at the bottom of the embankment along its centerline (D_v) ; h) permanent horizontal displacement of the foundation or embankment (D_h) ; i) peak transient horizontal displacement of the foundation or embankment (D_h) ; i) permanent foundation tilt (q) for all tests [NM, DGCs RF-DR, RF-DS, RF] during the Kobe-L motion. Note that the specific tests displayed in each subfigure may vary depending on the scenario under investigation; only reliable experimental values are included for comparison.

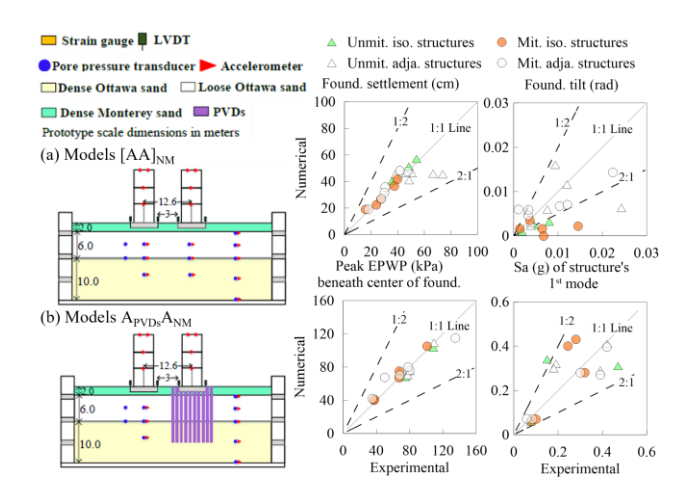


Fig. 5. Comparison of the experimental and numerical results for all neighboring structures in terms of permanent foundation settlement, permanent foundation tilt, peak EPWP beneath the center of foundation in the middle of the liquefiable layer, and foundation-level 5%-damped spectral acceleration at the structure's fundamental period.

Considering all sources of error and uncertainty in both

experimental and numerical models, the comparisons were considered satisfactory in capturing the key aspects of the seismic response of layered liquefiable deposits treated with DGCs near an embankment or a matfounded structure. We build on these numerical simulations next, to explore the role of additional variations in stratigraphy, mitigation properties, and ground motion characteristics on the performance of isolated and neighboring soil-structure systems treated with DGCs.

3 IMPACT OF MITIGATION ON PERFORMANCE OF ISOLATED STRUCTURES ON STRATIFIED SOILS

We conducted a limited numerical sensitivity study to evaluate the effectiveness of DGCs in mitigating the liquefaction hazard within stratigraphically variable liquefiable deposits and their impact on an isolated foundation and structure. We adjusted the soil profile, building characteristics, and DGC properties in this initial phase that is presented in the paper, while keeping the input ground motion consistent.

We examined five different soil configurations, as presented in Fig. 6. These profiles were inspired by variations typically observed in case histories with or without soil ejecta (Hutabarat and Bray 2021). These profiles included spatial variations in hydraulic conductivity, thickness, relative density, and continuity of critical layers. These soil profiles consisted of loose and dense layers of saturated Ottawa sand with $D_r = 40\%$ and 90%, representing the critical liquefiable and dense non-liquefiable layers, respectively. A surface layer of Monterey sand $(D_r = 90\%)$ was used as the dense draining crust. We introduced thin silica silt interlayers to disrupt critical layers' drainage capacity or continuity. These layers were assumed to have a thickness of 0.5 m with appropriately low permeability. Uniform, clean, fine gravel was used to represent the DGC material. The model parameters for all granular soil layers of interest were calibrated using prior studies (Badanagki et al. 2018; Hwang et al. 2021; Tiznado et al. 2021). The total height of all soil profiles was maintained at 24 m, and the water table depth (z_{gwt}) was set at 2 m. The dimensions of the soil domain were determined as 6 and 3 times the foundation width (width) in the x and ydirections, respectively (parallel and perpendicular to the shaking direction), based on Hwang et al. (2022). Additional variabilities associated with fines content and plasticity are beyond the scope of this paper but are highly recommended for future studies.

We evaluated two distinct structures referred to as A and B. Structure A was described previously. Structure B was added to represent a taller, heavier, and more flexible 9-story building (simplified with 2-DOFs) with an embedment depth (D_f) of 3 m representing a one-story basement (as previously detailed in Fig. 3c). In this sensitivity study, in addition to soil stratigraphy, we

varied the geometry and physical characteristics of the DGC known to be influential (e.g., based on Tiznado et al. 2021). These variables included the area replacement ratio (A_r) , the ratio of hydraulic conductivity of the DGC to that of the surrounding critical soil layer (k_r) , the ratio of the maximum shear modulus of the DGC to that of the surrounding critical soil layer (G_r) , and the densification of critical layers induced by DGC installation ($D_{r,DS}$). A_r was varied from 10% to 20%, in line with the available field case histories involving DGCs (Tiznado et al. 2020). G_r values ranged from 2 to 8, based on Baez (1995) and Tiznado et al. (2020). The selected values of k_r represented three extreme scenarios of DGC drainage capacity: complete clogging with fines ($k_r = 0$), clogging with the surrounding soil ($k_r = 1$) that would result in no change in drainage capacity, and no clogging with enhanced drainage ($k_r = 100$). Finally, $D_{r,DS}$ was estimated at 90% based on an initial $D_{r,c}$ of 40% and A_r values of 10% to 20%, following Baez (1995).

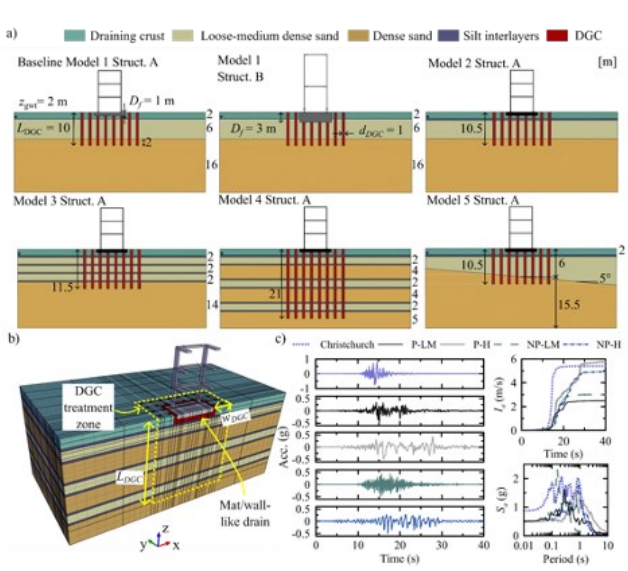


Fig. 6. a) Schematic view of the model configurations used in the numerical sensitivity study; b) Schematic view of a typical 3D numerical model simulating the response of a soil-foundation-structure system mitigated with DGCs for Model 4 and Structure A (all dimensions are in prototype meters); and c) Acceleration and Arias Intensity (I_a) time histories and 5%-damped acceleration response spectra (S_a) of the outcropping rock ground motions used as input in the numerical sensitivity study.

For all soil profiles, the depth of treatment (L_{DGC}) was designed to fully encompass the thickness of the critical layer(s), with an additional 2 m extension into the denser layer below. The range of L_{DGC} varied from 10 m to 21 m to cover the deepest critical layer(s), and the columns extended to the ground surface. The lateral extent of the treatment zone extended beyond the foundation edge by half of the foundation width (w_{DGC}) in both horizontal directions. When applicable, the zone of densification resulting from column installation was simplistically limited to the loose layers within the improved area. We used the maximum rotated horizontal component (RotD100) PGA from the 2011 Christchurch earthquake

recorded at the PARS station (detailed in Fig. 6c). This earthquake had a moment magnitude (M_w) of 6.0, and the site was located 3.6 km from the rupture source and classified as site class B. We performed deconvolution for each soil model to obtain the within-rock motion, which was used as input to the numerical model's rigid base.

To evaluate the effects of DGCs on the primary engineering demand parameters (EDPs) of interest, Fig. 7 presents the detailed numerical results obtained for a representative case (i.e., the baseline soil Model 1 and Structure A). This baseline model is characterized by a single uniform liquefiable layer with no silt interlayers and $z_{gwt} = 2$ m. The results include predictions of S_a at different locations, the roof-to-foundation and foundation-to-far-field spectral ratio, foundation δ , θ , lateral displacement (D_h) , r_u within the liquefiable layer, and roof flexural drift ratio time histories (per Karimi and Dashti 2016). We compare the "baseline" mitigation scenario, characterized by parameters $A_r = 10\%$, $k_r =$ 100, $G_r = 2$, $D_{r,c} = 40\%$, with the NM case. Furthermore, we explore the influence of varying DGC properties, as well as the impact of slightly varying the groundwater table depth (z_{gwt}) from 2 to 0 m in both NM and mitigated models.

Fig. 7 shows that the mitigation scenarios with enhanced drainage ($k_r = 100$), or all mitigation scenarios except $k_r = 0$) effectively reduced the amplitude and duration of r_u generation within the critical soil layer for this model, preventing liquefaction triggering (peak r_u of about 0.9). This r_u reduction subsequently decreased shear and volumetric deformations and the computed net δ compared to NM. The most substantial reduction in δ for $z_{gwt} = 2$ m (from $d_{NM} = 17$ cm to $d_{DGC} = 8$ cm, i.e., δ_{DGC}/δ_{NM} = 0.45) was achieved when considering both enhanced drainage and installation-induced densification ($D_{r,DS} = 90\%$). However, in cases where clogging occurred ($k_r = 0$ or 1), DGCs did not yield substantial improvements in δ , primarily due to lower dissipation rates and increased r_u values after strong shaking compared to NM.

Fig. 7 also revealed that enhanced drainage $(k_r =$ 100), while successfully reducing settlement, slightly amplified the foundation's transient rotation and had a minor impact on permanent tilt. The baseline mitigation scenario, as well as cases with $G_r = 8$ and $D_{r,DS} = 90\%$, only provided minor reductions in permanent tilt compared to the NM case. Significant acceleration amplification from the foundation to the roof was observed near the structure's fundamental period (i.e., $T_{o,StrA} = 0.56$ s) and the motion's mean period ($T_m = 0.63$ s) with or without mitigation. In these cases, T_m also closely aligned with both $T_{o,StrA}$ and T_{so} (initial smallstrain fundamental period of the site ~ 0.49 s [for the NM case]), which led to resonance within the soil-structure system. Draining DGCs amplified the seismic demand within the liquefiable layer and on the foundation and

roof compared to NM. This S_a amplification occurred for most DGC scenarios on the roof near the first two modes of Structure A ($T_{o,StrA}$ = 0.56 s and 0.19 s) and on the foundation or liquefiable layer at shorter periods (from 0.01 to 0.2 s), due to reduced damping and increased overall shear stiffness within the treated soil, particularly when drainage was combined with densification ($D_{r,DS}$ = 90%). Additionally, DGCs slightly amplified peak and permanent flexural drifts due to the increased foundation transverse accelerations. These amplifications are important to consider in structural design.

Finally, reducing the depth to the groundwater table (z_{gwt}) from 2 to 0 m increased δ_{NM} of Structure A by approximately 75%. This increase is due to reduced effective normal stresses beneath the foundation and increased softening and damping within the soil at shallower depths. Consequently, this change also slightly de-amplified the accelerations transmitted to the superstructure. Implementing DGCs for this z_{gwt} reduced the normalized foundation settlement (δ_{DGC}/δ_{NM}) to 0.42. In the context of SSI, conventional foundation design approaches rely on free-field surface accelerations as the primary input. Alternatively, design guidelines commonly suggest attenuating accelerations at shorter periods to account for kinematic constraints associated with embedded foundations or base slab averaging. As shown in Fig. 7, short-period (i.e., 0.01-0.5 s) foundation-to-far-field spectral ratios were highly sensitive to the presence and properties of mitigation. Generally, the reductions in low period foundation-freefield spectral ratios are minor on liquefiable sites. The addition of DGCs (particularly draining DGCs with adjacent ground densification) had the potential to notably amplify the accelerations on the foundation at shorter periods up to a factor of about 3.

Fig. 8 shows the peak r_u and shear strain ($r_{u,max}$, and γ_{max}) profiles with depth for all soil models, isolated structures, and mitigation scenarios considered in this paper. In models with thick and continuous liquefiable layers (i.e., $H_{crit} = 6$ m, Models 1, 2, and 5), draining DGCs proved highly effective in reducing $r_{u,max}$ and γ_{max} (and hence, triggering and strength loss) within the loose sand layer compared to NM, consistent with Tiznado et al. (2021) observations in the far-field. The most pronounced reduction in $r_{u,max}$ was observed when drainage was combined with densification ($D_{r,DS}$ = 90%); the case with larger $A_r = 20\%$ also showed a pronounced reduction. For example, $r_{u,max}$ ranged from 0.9 to 1.0 for NM and 0.4 to 0.65 with draining DGCs in Models 1, 2, and 5. However, the same models mitigated with clogged DGCs ($k_r = 0$ or $k_r = 1$) did not experience a major change in $r_{u,max}$, and γ_{max} .

The presence of low-permeability silt interlayers that interrupted the continuity of the critical layers and restricted vertical water flow (i.e., Models 3-4) limited the effectiveness of draining DGCs in reducing $r_{u,max}$ under both structures compared to Models 1, 2, and 5

($r_{u,max}$ ranging from 0.6 to 1.0 with DGCs), even at depths as large as 17 m. Substantial γ_{max} values were also predicted within the critical layers in Models 3-4 with DGCs, at times exceeding NM in shallow layers when clogged ($k_r = 0$ or 1). In Model 4, large $r_{u,max}$, γ_{max} , and softening in a deeper critical layer reduced the seismic demand and strains at shallow depths (similar to a base isolation effect), both with or without mitigation. DGCs in Model 4 redistributed the excess pore water pressures and shear strains from shallow critical soil layers to a greater share in thicker, denser layers with an extended duration.

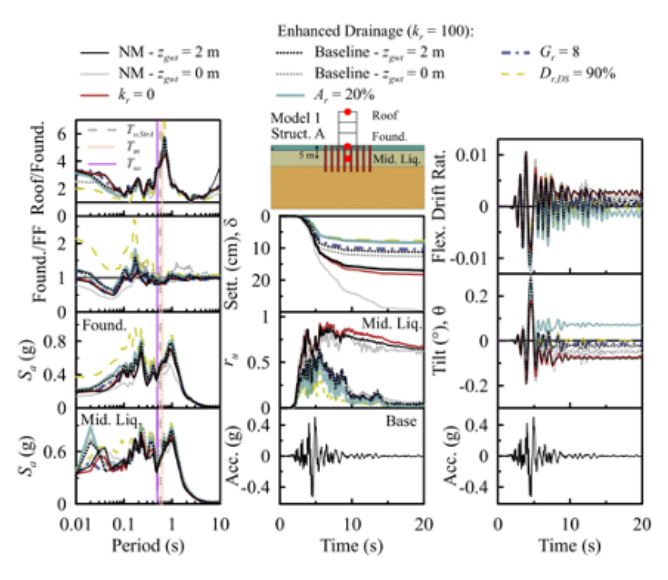


Fig. 7. Key results for baseline soil profile, unmitigated and mitigated cases showing: 5%-damped acceleration response spectra (S_a) at different locations, foundation settlement (δ) , excess pore water pressure ratio (r_u) time histories (EPWP) in the middle of the critical layer, roof flexural drift ratio, tilt (θ) , and foundation lateral displacement (D_h) , as a function of dense granular column properties and water table depth.

Structure B's greater confining pressure reduced $r_{u,max}$ in critical layers for all NM and DGC cases compared to A. Additionally, silt interlayers in Models 2-5 increased $r_{u,max}$, and γ_{max} directly below the foundation of Structure A, whereas the deeper embedment of Structure B reduced those effects. As for the far-field response (obtained from the NM model), the reduced confinement compared to the near-field soil increased the accumulation of shear strains within the critical layers.

Continuum models cannot capture the formation and effects of soil ejecta on deformations. There are also no well-established empirical methods for estimating settlement resulting from the ejection of sand to the surface, in the far-field or near-field. In our study, we employ the Ejecta Potential Index (EPI) in combination with the severity classes proposed by Hutabarat et al. (2021) to offer insights into the potential reduction in ejecta severity under the building's center (UB) with different DGC scenarios. This metric has been shown to

correlate well with previous field observations of surface ejecta (though only evaluated in the free-field in prior studies from Christchurch). The concept underlying EPI involves monitoring the duration during which the numerically computed excess hydraulic head ($h_{exc} = Du/g_w$) exceeds the hydraulic head required for artesian flow. Fig. 9 compares the computed EPI_{UB} under the building's confining pressure with different mitigation scenarios together with the ejecta severity classes. Unmitigated soil deposits all led to an ejecta severity class of "extreme" due to the shallow depth of the groundwater table ($z_{gwt} = 2$ m).

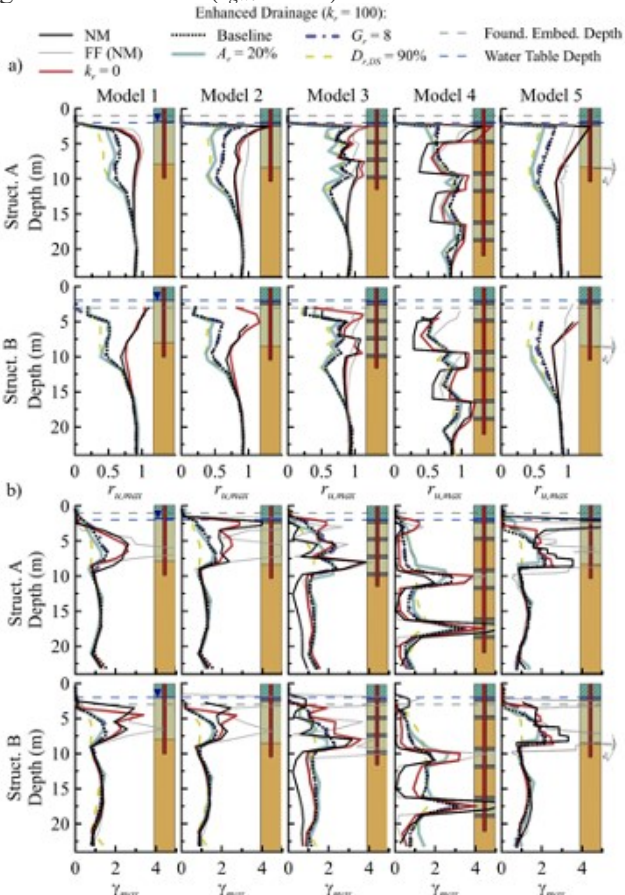


Fig. 8. a) Peak excess pore pressure ratio ($r_{u,max}$) and b) maximum shear strain (g_{max}) with depth under the center of structures compared to the far-field (obtained from NM model) as a function of DGC properties and structure, compared with a model with no mitigation (NM), a baseline mitigation scenario (Baseline, where $A_r = 10\%$, $k_r = 100$, $G_r = 2$, and $D_{r,c} = 40\%$).

The results highlight the notable impact of draining DGCs in reducing the severity of ejecta potential under both foundations. Following the ejecta severity thresholds established by Hutabarat et al. (2021), draining and reinforcing DGCs with $D_{r,DS} = 90\%$ was the most effective approach in reducing the ejecta severity class from "extreme" (for NM) to "none". On the other end of the spectrum, the baseline mitigation case showed essentially no improvement in EPI.

Fig. 10 offers insights into the effectiveness of various DGC mechanisms for the conditions

investigated on EDPs of interest. We compare the median. minimum, and maximum normalized EDP_{DGC}/EDP_{NM} predictions from the five soil models for each structure for $z_{gwt} = 2$ m, along with their respective absolute values (NM or DGC), to evaluate the effect of stratigraphic variability on DGC performance. The results highlight the effectiveness of draining DGCs $(k_r = 100)$ in reducing δ compared to NM across the range of soil profiles, geometries, and structures. For example, the median value of δ_{DGC}/δ_{NM} ranged from 0.66 (baseline scenario) to 0.45 ($D_{r,DS} = 90\%$) for both structures, with a mean of 0.54. Fig. 10a shows that the median permanent foundation settlement of different mitigation scenarios ranged from 2 cm (acceptable) to 31 cm (well above the design limit) due only to changes in soil stratigraphy, with most failing to meet the design threshold of 5 cm. For Models 1-3 and 5 under both structures, DGCs generally reduced δ with median δ_{DGC}/δ_{NM} ranging from 0.28 to 0.78 (mean = 0.52). Introducing thin silt interlayers above continuous critical liquefiable layers (i.e., Models 2 and 5) resulted in larger δ_{NM} values for both structures due to slower excess pore pressure dissipation. However, draining DGCs ($k_r = 100$) generally improved these soil deposits with median $\delta_{DGC}/\delta_{NM} = 0.30 - 0.53$, as drain extensions through the silt cap expedited excess pore pressure dissipation.

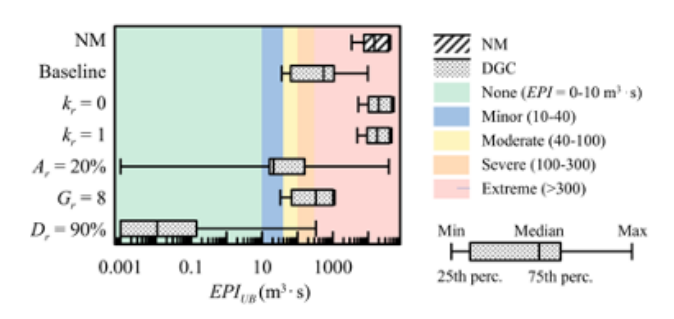


Fig. 9. Comparison of EPI_{UB} under the center of the building with the ejecta severity classes proposed by Hutabarat et al. (2021) compared with an unmitigated model (NM) and a baseline mitigation scenario (Baseline, where $A_r = 10\%$, $k_r = 100$, $G_r = 2$, and $D_{r,c} = 40\%$), as a function of dense granular column properties for all soil models and structures.

Fig. 10a also highlights the distinct behavior of mitigation in Model 4 with multiple, separated critical loose sand layers. This soil profile exhibited base isolation resulting from substantial soil softening in the deepest critical layers, reducing permanent foundation settlement of NM compared to the design limit and other soil profiles. However, Model 4 was the only case where DGCs increased the settlement relative to the NM case. This settlement increase was primarily due to EPWP migration toward denser layers and the increase in pore pressures and shear strains over an extended period of time within a larger volume of soil.

Importantly, Fig. 10b,c show that the effect of DGCs on foundation tilt strongly depends on the properties of

the structure. In the case of Structure A, mitigation slightly increased permanent tilt compared to NM, particularly with clogged drains $(k_r = 0, 1)$. We hypothesize that this amplification is due to increased pore pressures in the underlying soil treated with clogged DGCs. This highlights the importance of installing adequate filters around the drains to prevent clogging to the extent possible. However, predicted tilts are generally negligible (i.e., permanent $\theta_{NM} = 0.01 - 0.08^{\circ}$ for Models 1-4 [see Fig. 10b], aligning with expected values for isolated structures on uniform liquefiable layers reported in Bullock et al. 2019b). These changes in tilt become more important in urban settings involving asymmetric stress states (see the following section). Consequently, the observed tilt values with or without DGCs for Structure A in Models 1-4 might be well within the scatter and uncertainty expected for such small demand parameters. In Model 5 with Structure A, the non-uniform liquefiable layer increased shear strain accumulation downslope, encouraging greater tilt compared to other soil profiles. In this case, the permanent $\theta_{NM-StrA}$ reached up to 0.8°, surpassing the design threshold (i.e., 0.2°). Fig. 10b shows that DGCs effectively reduced the foundation's permanent tilt in Model 5 with Structure A by reducing the accumulation of asymmetric seismic deformations beneath the foundation.

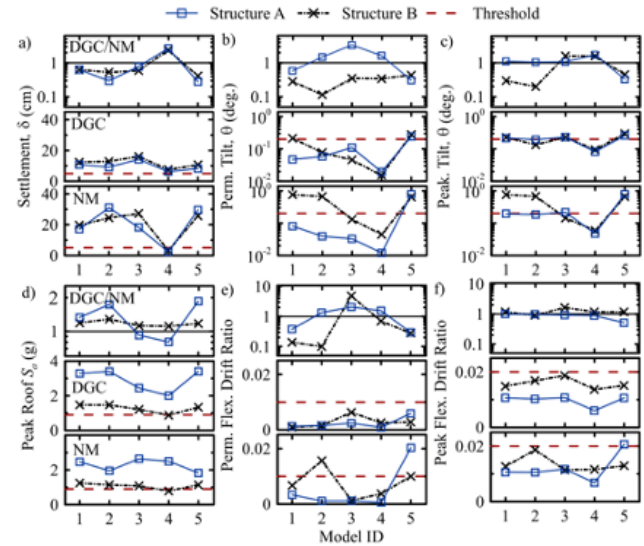


Fig. 10. Median normalized (ratio of mitigated to unmitigated) response, mitigated response (with DGCs), and response with no mitigation (NM) for different models in terms of: a) permanent foundation settlement (δ); b) permanent foundation tilt (θ); c) peak transient θ ; d) peak roof 5%-damped S_a ; e) permanent roof flexural drift ratio; and f) peak transient roof flexural drift ratio compared with design limits. The figure presents the median predictions from the six mitigation configurations for each structure.

Fig. 10b shows a decrease in NM permanent foundation tilt in Models 3-4 for both structures compared to Model 1. This reduction can be attributed to reduced continuity and thickness of the liquefiable layers

in Models 3-4. In these cases, thinner liquefiable layers (particularly when further from the foundation's influence zone) can decrease the accumulation of large asymmetric strains beneath the foundation compared to more shallow and thick critical layers, promoting a more stable foundation response. Overall, the results indicate that mitigation effectiveness is highly sensitive to the properties and geometry of the soil profile, structure, foundation, and the active mechanism of mitigation.

4 IMPACT OF MITIGATION ON PERFORMANCE OF ADJACENT STRUCTURES

The response of two adjacent structures like A was evaluated on two soil Models 1 and 2 in this preliminary investigation, at spacings ranging from 1.5 to 6 m. All models of SSSI presented in this paper included fully draining DGCs (with no densification) around one in a pair of two buildings. Fig. 11 shows a schematic of simulations involving two adjacent buildings. representing conditions expected at the corner or edge of a cluster. The same base motion was used as shown previously for isolated structures. Fig. 12 shows the shear strain contours obtained around the two structures, showing that DGCs successfully reduced shear deformations around the mitigated structure as well as the inner edge of the unmitigated neighbor, particularly at the shorter spacing of 1.5 m.

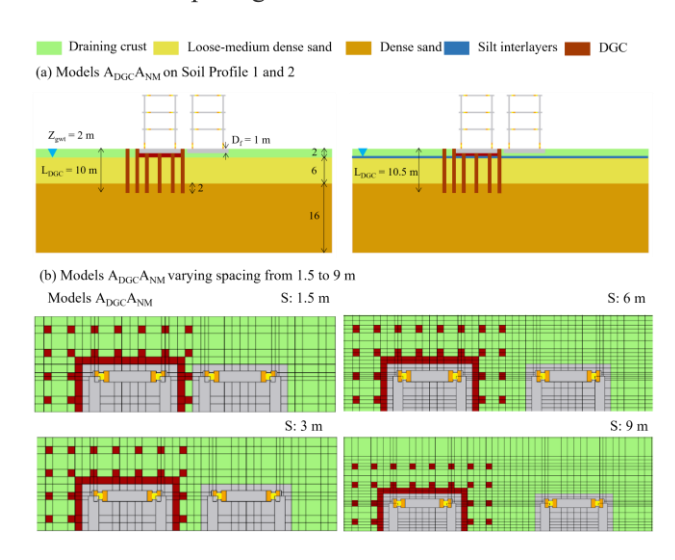
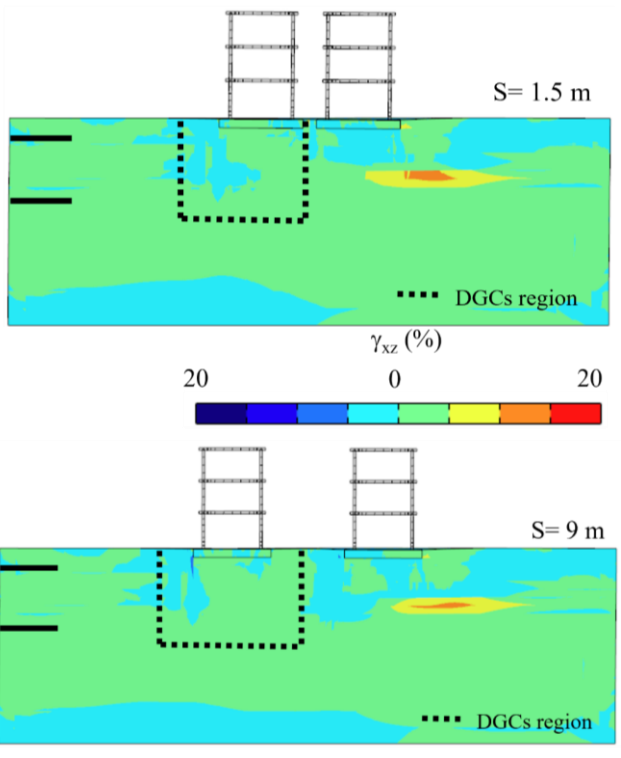


Fig. 11. a) Schematic view of the model configurations used in the numerical sensitivity study involving SSSI; b) Top view of the SSSI models varying foundation's edge-to-edge spacings (S).

Fig. 13 shows the contours of effective vertical stress in $A_{DGC}A_{NM}$ with a spacing of 1.5 and 9 m on soil Models 1 and 2 at the end of shaking, as representative examples. In-plane shear stresses were reduced between the two foundations at shorter spacings. However, larger out-of-plane shear and vertical stresses below foundations' inner edges encouraged greater accumulations of soil strains and deformations in soils between two foundations under prolonged soil softening.

These biases significantly amplified the tilt response of both unmitigated and mitigated structures under SSSI at shorter spacings compared to isolated SSI, particularly for models involving a thin silt layer (Profile 2).

(a) Models A_{DGC}A_{NM} on soil profile 1



(b) Models A_{DGC}A_{NM} on soil profile 2

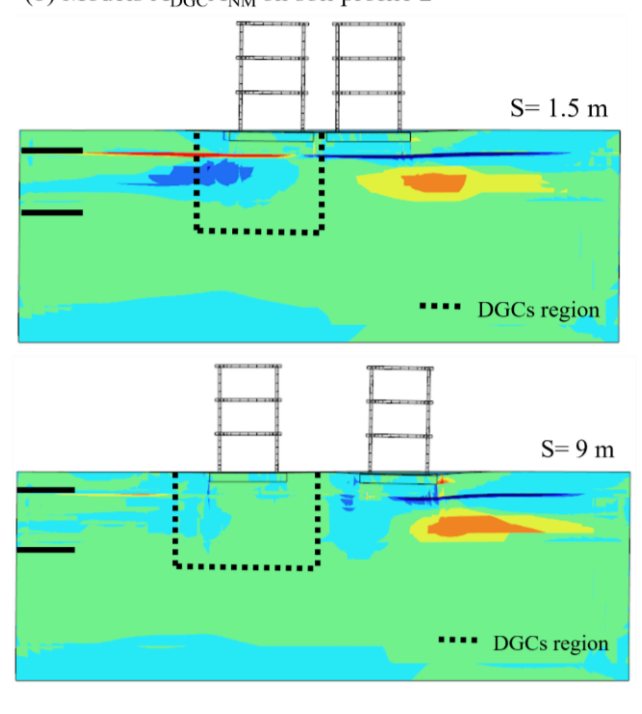


Fig. 12. The contours of accumulated shear strain in $A_{DGC}A_{NM}$ with a spacing (S) of 1.5 and 9 m on soil Models 1 and 2 at the end of shaking.



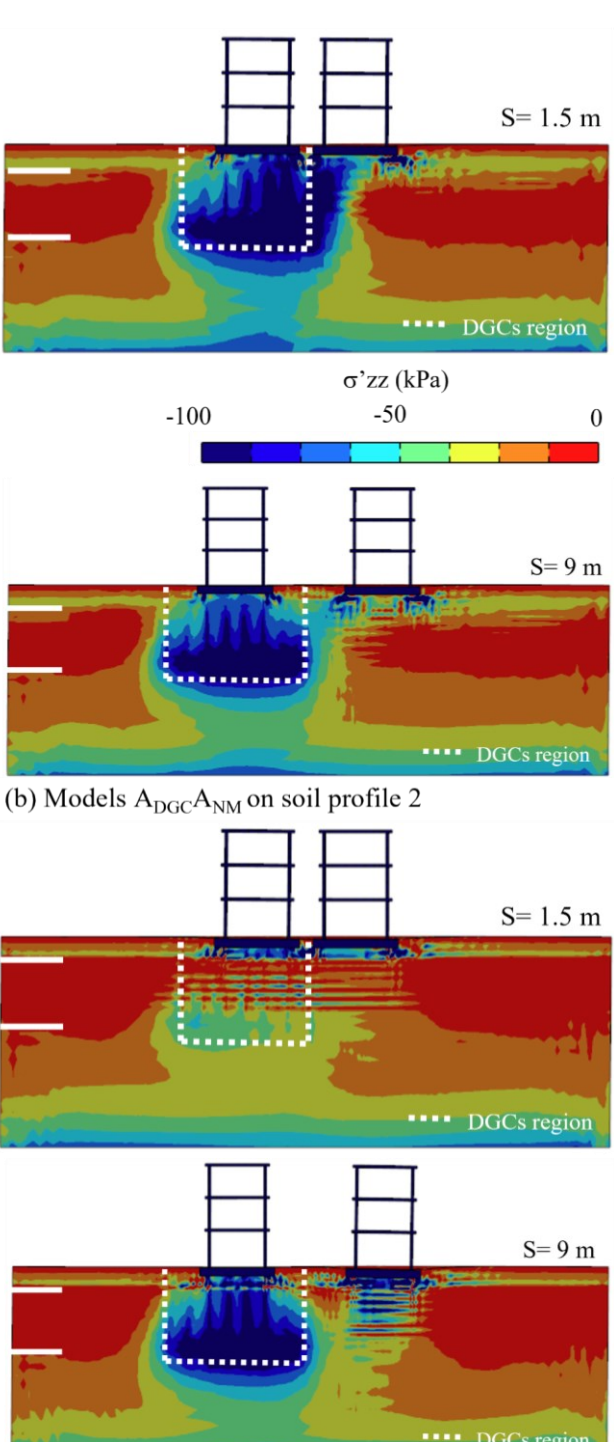


Fig. 13. The contours of effective vertical stress in $A_{\rm DGC}A_{\rm NM}$ with a spacing of 1.5 and 9 m on soil Models 1 and 2 at the end of shaking.

The simulations performed for different spacing-to-foundation width-ratios (S/W) on soil Models 1 and 2 are presented in Fig. 14. In the model that included only uniform sand layers (Model 1), DGCs substantially reduced the settlement of the mitigated structure for S/W

ranging from 0 to 1, though still not to acceptable levels. The settlement of mitigated Structure A generally reduced at larger spacings. Use of DGCs around one structure simultaneously slightly amplified settlement of the unmitigated neighbor, by amplifying the drainage rate near its foundation. The presence of a thin silt layer in Model 2 with SSSI drastically reduced the settlement efficacy of DGCs at S/W < 0.3 compared to the case of an isolated building (SSI). At shorter spacings between the neighboring structures, an increase in drainage path was expected in soils below the foundations, leading to a greater extent of soil softening. This is manifested in terms of reduced vertical effective stresses below the foundations at shorter spacings at the end of shaking in Fig. 13b. Note, also, that in Model 2, the presence of silt notably amplified the degree of softening and EPWPs, reducing the effective stresses below the mitigated structure at the end of shaking. The combined effect of silt interlayer and SSSI on the DGC's settlement efficacy became negligible at S/W > 0.3.

SSSI was generally observed to increase the rotation of both neighboring structures at S/W < 1, with or without mitigation (by a factor up to about 50). The presence of a thin silt layer in Model 2 together with DGCs around one in the pair further amplified the tilt of the adjacent unmitigated neighbor at S/W between 0.3 and 1. The DGCs reduced the EPWPs and amplified effective stresses during shaking below the inner edge of the unmitigated neighbor. This increased the degree of asymmetry and bias in the shear stiffness and accumulation of shear strains between the two edges of its foundation. This effect was visible for S/W up to 1.0.

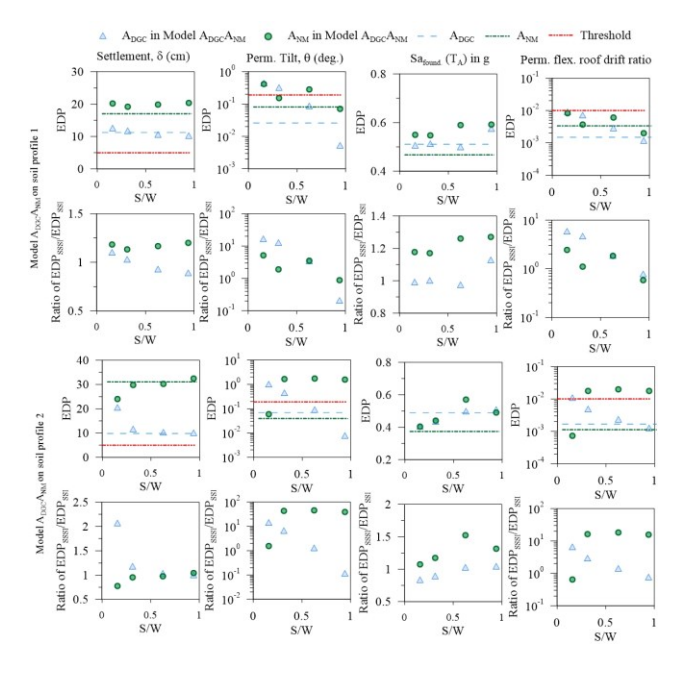


Fig. 14. Mitigated response (with DGCs) and response with no mitigation (NM) for different models in terms of permanent foundation settlement (δ), permanent foundation tilt (θ), 5%-damped Foundation S_a at Structure A's natural period, permanent roof flexural drift ratio.

SSSI generally amplified the spectral accelerations at the foundation and flexural drifts within the superstructure of the neighboring unmitigated building in both soil profiles. In Model 1, the flexural drifts stayed within the allowed design limit for models considering either SSI or SSSI. The silt layer in Model 2 pushed the flexural drifts within the unmitigated neighbor to values slightly greater than the design level, indicating plastic deformations and damage within the superstructure, particularly for models involving SSSI. The increase in flexural drift amplified foundation's overturning moment (due to P- Δ effects), and hence its cumulative rotation. In general, the combined influence of SSSI and stratigraphic variability on mitigation efficacy are shown to be significant in terms of foundation tilt, spectral accelerations, and drifts, particularly on the unmitigated neighbor at S/W as large as 1.0. Additional stratigraphic variability (for example Model configurations 3-5 in Fig. 6) are expected to lead to even greater amplifications in the key EDPs of interest under SSSI, which is alarming in terms of mitigation efficacy. Additional measures may be needed to reduce tilt to acceptable levels in urban settings and with realistically stratified deposits, while simultaneously improving the ground and strengthening the superstructures at an area-level.

5 CONCLUDING REMARKS AND PRACTICAL IMPLICATIONS

Due to the significant impacts and environmental justice implications of community relocation in areas with a high likelihood of seismic liquefaction, it is prudent to reliably assess the efficacy of area-wide mitigation at a systems level. The existing engineering methodologies for liquefaction mitigation still rely on free-field triggering in uniformly layered profiles of granular soils. These methods often do not account for cross-layer interactions in stratified soil profiles, the consequences of liquefaction or mitigation on the performance and damage potential of the foundationstructure system, or the interactions between and among multiple structures in close proximity of each other. Hence, these methods are unreliable, particularly in urban settings. Unreliable assessment of hazard and consequence tampers reliable risk estimation and decision making regarding mitigation. This leaves many major cities in seismically active areas and their most marginalized communities at risk of liquefaction related damage or relocation.

In this paper, we first use centrifuge experiments to evaluate the ability of 3D, fully-coupled, dynamic finite-element analyses with a state-of-the-art soil constitutive model in capturing the seismic response of stratified liquefiable deposits and foundation-structure systems mitigated with dense granular columns (DGCs). DGCs are selected for this study, as they cover a range of expected mitigation mechanisms, through drainage, reinforcement, and densification. A limited sensitivity

study follows, where we more comprehensively and systematically evaluate how DGC mitigation, stratigraphic variability, building properties, and seismic coupling between neighboring buildings affect mitigation efficacy in terms of the EDPs of interest.

The results generally indicate improved foundation performance in terms of settlement (though not to acceptable design levels) with DGCs that combined enhance drainage and installation-induced densification. The only exception was in cases involving deeper liquefiable deposits that lead to base isolation, where DGCs could in fact worsen foundation settlements. The DGCs are shown to potentially amplify foundation tilt, depending on structural properties and stratigraphic variations of the site, particularly in cases where DGCs are clogged. This observation points to the critical importance of minimizing clogging potential during construction. The potential increase in foundation tilt, which can be significant, must be evaluated on a caseby-case basis, particularly when on stratified deposits and near other buildings in a cluster.

In general, the combined influence of SSSI and stratigraphic variability on mitigation efficacy is shown to be significant in terms of foundation tilt, spectral accelerations, and drifts, particularly on the unmitigated neighbor at S/W as large as 1.0. This highlights the significance of considering seismic coupling between and among structures in a cluster in urban settings as well as detailed characterization of interlayering and stratigraphy. Additional measures and technologies may be needed to reduce tilt to acceptable levels in closelyspaced cluster configurations with asymmetric stress states, while simultaneously strengthening both the ground and structures at an area-wide level. Such a community-based approach to liquefaction mitigation, however, will introduce new planning and legal challenges that require further investigation in the future.

ACKNOWLEDGEMENTS

This work was supported by the National Science Foundation (NSF) under grant no. 2135669 and the Natural Sciences and Engineering Research Council of Canada (NSERC). All statements in this paper are those of the authors and do not necessarily reflect the views of the funding agencies. This work utilized the Alpine high-performance computing resource at the University of Colorado Boulder. Alpine is jointly funded by the University of Colorado Boulder, the University of Colorado Anschutz, Colorado State University, and the National Science Foundation (award no. 2201538).

REFERENCES

Baez, J. I. (1995). "A design model for the reduction of soil liquefaction by 1200 vibro-stone columns." *Ph.D. Dissertation*, Dept. of Civil and Environmental 1201 Engineering, Univ. of Southern California.

Badanagki, M., Dashti, S., Paramasivam, B., Tiznado,

J.C. (2019). "How Do Granular Columns Affect the Seismic Performance of Non-Uniform Liquefiable Sites and Their Overlying Structures?" Soil Dynamics and Earthquake Engineering, 125.

Badanagki, M., Dashti, S., Kirkwood, P. (2018). "An Experimental Study of the Influence of Dense Granular Columns on the Performance of Level and Gently Sloping Liquefiable Sites," ASCE Journal of Geotechnical and GeoEnvironmental Engineering, 144(9), https://doi.org/10.1061/(ASCE)GT.1943-5606.0001937.

Balachandran, Olshansky, and Johnson (2021). "Planning for Disaster Induced Relocation of Communities," Journal of the American Planning Association, Vol. 88, No. 3.

Beyzaei, C. Z., Bray, J. D., van Ballegooy, S., Cubrinovski, M., & Bastin, S. (2018). "Depositional environment effects on observed liquefaction performance in silt swamps during the Canterbury earthquake sequence." *Soil Dynamics and Earthquake Engineering*, 107, 303-321.

Bullock, Z., Karimi, S., Dashti, S., Porter, K., Liel, A., Franke, K. (2019a). "A Physics-Informed Semi-Empirical Probabilistic Model for the Settlement of Shallow-Founded Structures on Liquefiable

Ground," Géotechnique, https://doi.org/10.1680/jgeot.17.P.174.

Bullock, Z., Dashti, S., Karimi, Z., Liel, A., Porter, K., Franke, K. (2019b). "Probabilistic Models for the Residual and Peak Transient Tilt of Mat-Founded Structures on Liquefiable Soils," ASCE Journal of Geotechnical and GeoEnvironmental Engineering, 145(2).

Cabas, A., Lorenzo-Velazquez, C., Abayo, N.I., Ji, C., Ramirez, J., Garcia, F.E., Perodin, J., Hwang, Y.W., Dashti, S., Ganapati, N.E., Nicolas, S., Whitworth, M.R.Z. Guerrier, K., Fleur, N.S., Contreras, S., Largesse, R., Marcelin, L.H., Remington, C.L. (2023). "Intersectional impacts of the 2021 Mw 7.2 Nippes, Haiti, Earthquake from Geotechnical and Social Perspectives," *Bulletin of the Seismological Society of America* (BSSA), https://doi.org/10.1785/0120220118.

Cubrinovski, M., Rhodes, A., and Ntritsos, N. (2017). "System response of liquefiable deposits." 3^{rd} Int. Conf. on Performance-based Design in Earthquake Geotechnical Engineering, Vancouver, Canada.

Dashti, S., Ganapati, N.E., Abayo, N.I., Cabas, A., Calderon, J.R., Contreras, S., Desssable, J.E., Garcia, E., Guerrier, K., Hwang, Y.W., Jeannot, T., Ji, C., Lagesse, R., Logiste, M., Lorenzo-Velazquez, C., Nicolas, S., Remington, C., Perodin, J., Saint Fleur, N. Shriro, M., Vissiere, S., Whitworth, M. (2022). "Reconnaissance Following the August 14, 2021 Haiti Earthquake: Perspectives from Geotechnical Engineering and Social/Political Sciences," Geotechnical Extreme Event Reconnaissance (GEER) Report. doi:10.18118/G60090.

Dashti, S., Bray, J., Pestana, J., Riemer, M., and Wilson, D. (2010a). "Mechanisms of seismically induced settlement of buildings with shallow foundations on liquefiable soil." *J. Geotech. Geoenviron. Eng.*, 136(1), 151-164.

Dashti, S., Bray, J., Pestana, J., Riemer, M., and Wilson, D. (2010b). "Centrifuge testing to evaluate and mitigate liquefaction-induced building settlement mechanisms." *J. Geotech. Geoenviron. Eng.*, 136 (7), 918-929.

Elgamal, A., Z. Yang, and E. Parra (2002). "Computational modeling of cyclic mobility and post liquefaction site response," *Soil Dyn. Earthquake Eng.*, 22 (4): 259–271. https://doi.org/10.1016/S0267-7261(02)00022-2.

Hausler, E. A. (2002). "Influence of ground improvement on

settlement and liquefaction: A study based on field case history evidence and dynamic geotechnical centrifuge tests." *Ph.D. Dissertation*, Dept. of Civil and Environmental Engineering, Univ. of California at Berkeley.

Hutabarat, D., Bray, J.D. (2021). "Effective stress analysis of liquefiable sites to estimate the severity of sediment ejecta," *Journal of Geotechnical and GeoEnvironmental Engineering*, 147(5).

Hwang, Y.W., Dashti, S.⁺, Kirkwood, P. (2022). "Impact of Ground Densification on the Response of Urban Liquefiable Sites and Structures," *ASCE Journal of Geotechnical and GeoEnvironmental Engineering*, DOI: 10.1061/(ASCE)GT.1943-5606.0002710.

Hwang, Y.W., Ramirez, J., Dashti, S., Kirkwood, P., Liel, A.B., Camata, G., Petracca, M. (2021). "Seismic Interaction of Adjacent Structures on Liquefiable Soils: Insight from Centrifuge and Numerical Modeling," *ASCE Journal of Geotechnical Engineering and Geomechanics*, 147(8).

Ishihara, K. (1985). "Stability of natural deposits during earthquakes." *Proc., 11th Int. Conf. on Soil Mechanics and Foundation Engineering*, A. A. Balkema Publishers, Rotterdam, The Netherlands, 321-376.

Karimi, Z., and Dashti, S. (2016). "Seismic Performance of Shallow Founded Structures on Liquefiable Ground: Validation of Numerical Simulations Using Centrifuge Experiments," Journal of Geotechnical and Geoenvironmental Engineering, ASCE, 10.1061/(ASCE)GT.1943-5606.0001479.

Karimi, Z., Dashti, S., Bullock, Z., Porter, K., Liel, A. (2018). "Key Predictors of Structure Settlement on Liquefiable Ground: A Numerical Parametric Study," *Soil Dynamics and Earthquake Engineering*, 113, 286-308, DOI: https://doi.org/10.1016/j.soildyn.2018.03.001.

Kirkwood, P., and Dashti, S.⁺ (2019). "Influence of Prefabricated Vertical Drains on the Seismic Performance of Similar Neighboring Structures Founded on Liquefiable Deposits," *Geotechnique*, DOI: https://doi.org/10.1680/jgeot.17.

Kirkwood, P., and Dashti, S.⁺ (2018a). "A Centrifuge Study of Seismic Structure-Soil-Structure Interaction on Liquefiable Ground and the Implications for Structural Performance," *Earthquake Spectra*, 34(3), 1-22, DOI: 10.1193/052417EOS095M.

Kirkwood, P., and Dashti, S.⁺ (2018b). "Considerations for Mitigation of Earthquake-Induced Soil Liquefaction in Urban Environments," *ASCE Journal of Geotechnical and GeoEnvironmental Engineering*, 144(10), DOI: 10.1061/(ASCE)GT.1943-5606.0001936.

Kokusho, T., and Fujita, K. (2001). "Water films involved in post-liquefaction flow failure in Niigata City during the 1964 Niigata earthquake." *Proc., Fourth Int. Conf. on Recent Advances in Geotechnical Earthquake Engineering and Soil Dynamics*, Univ. of Missouri-Rolla, Rolla, Mo.

Li, P., Dashti, S., Badanagki, M., Kirkwood, P. (2018). "Evaluating 2-D Numerical Simulations of Dense Granular Columns in Level and Gently Sloping Liquefiable Sites using Centrifuge Experiments," *Soil Dynamics and Earthquake Engineering*, 110, 232-243.

Luque, R. and Bray, J.D. (2017). "Dynamic analyses of two buildings founded on liquefiable soils during the Canterbury earthquake sequence," *ASCE Journal of Geotechnical and GeoEnvironmental Eng.*, 143(9), DOI: 10.1061/(ASCE)GT.1943-5606.0001736.

Mazzoni, S., McKenna, F., Scott, M. H., Fenves, G. L. (2006). "Open System for Earthquake Engineering Simulation (OpenSees) Command Language Manual," Berkeley, CA: Network for Earthquake Engineering Simulations.

NCEER (1997). "Proceedings of the NCEER Workshop on Evaluation of Liquefaction Resistance of Soils," Edited by Youd, T.L., Idriss, I.M., *Technical Report* No. NCEER-97-0022, December 31, 1997.

Olarte, J., Dashti, S., Liel, L. (2017). "Can Ground Densification Improve Seismic Performance of Inelastic Structures on Liquefiable Soils?" *Journal of Earthquake Engineering and Structural Dynamics*, DOI: 10.1002/eqe.3012.

O'Rourke, T.D. and Lane, P.A. (1989). "Liquefaction Hazards and Their Effects on Buried Pipelines," *National Center for Earthquake Engineering Research*, Technical Report NCEER-89-0007.

Paramasivam, B., Dashti, S., Liel, A. (2019). "Impact of Spatial Variations in Permeability of Liquefiable Deposits on the Seismic Performance of Structures and Effectiveness of Drains," ASCE Journal of Geotechnical and GeoEnvironmental Engineering, 145(8).

Ramirez, J., Barrero, A., Chen, L., Dashti, S.+, Ghofrani, A.,

Taiebat, M., Arduino, P. (2018). "Site Response in a Layered Liquefiable Deposit: Evaluation of Different Numerical Tools and Methodologies with Centrifuge Experimental Results," *ASCE Journal of Geotechnical and GeoEnvironmental Engineering*, 144(10), https://doi.org/10.1061/(ASCE)GT.1943-5606.0001947.

Rayamajhi, D., Ashford, S. A., Boulanger, R. W., and Elgamal, A. (2016a). "Dense granular columns in liquefiable ground. I: Shear reinforcement and cyclic stress ratio reduction." *J. of Geotechnical and GeoEnvironmental Eng.*, 142 (7): 4016023.

Rayamajhi, D., Boulanger, R. W., Ashford, S. A., and Elgamal, A. (2016b). "Dense granular columns in liquefiable ground. II: effects on deformations." *J. of Geotechnical and GeoEnvironmental Eng.*, 142 (7): 04016024.

Tiznado, J.C., Dashti, S.⁺, Ledezma, C. (2021). "A Probabilistic Predictive Model for Liquefaction Triggering in Layered Sites Improved with Dense Granular Columns," *ASCE Journal of Geotechnical and GeoEnvironmental Engineering*, DOI: 10.1061/(ASCE)GT.1943-5606.0002609.

Tiznado, J.C., Dashti, S.⁺, Ledezma, C., Wham, B. (2020). "Performance of Embankments on Liquefiable Soils Improved with Dense Granular Columns: Observations from Case Histories and Centrifuge Experiments," *ASCE Journal of Geotechnical and GeoEnvironmental Engineering*, 146(9).